Monolayer MoS_2 Heterojunction Solar Cells

Meng-Lin Tsai,[†,⊥] Sheng-Han Su,[‡,§] Jan-Kai Chang,[‡] Dung-Sheng Tsai,[‡] Chang-Hsiao Chen,[§] Chih-I Wu,[‡] Lain-Jong Li,[§,⊥] Lih-Juann Chen,[†,*] and Jr-Hau He[‡,⊥,*]

[†]Department of Materials Science and Engineering, National Tsing Hua University, Hsinchu 30013, Taiwan, [‡]Institute of Photonics and Optoelectronics & Department of Electrical Engineering, National Taiwan University, Taipei 10617, Taiwan, [§]Institute of Atomic and Molecular Sciences, Academia Sinica, Taipei 11529, Taiwan, and [⊥]Computer, Electrical and Mathematical Sciences and Engineering (CEMSE) Division, King Abdullah University of Science & Technology (KAUST), Thuwal 23955-6900, Saudi Arabia

ABSTRACT We realized photovoltaic operation in large-scale MoS_2 monolayers by the formation of a type-II heterojunction with p-Si. The MoS_2 monolayer introduces a built-in electric field near the interface between MoS_2 and p-Si to help photogenerated carrier separation. Such a heterojunction photovoltaic device achieves a power conversion efficiency of 5.23%, which is the highest efficiency among all monolayer transition-metal dichalcogenide-based solar cells. The demonstrated results of monolayer MoS_2/Si-based solar cells hold the promise for integration of 2D materials with commercially available Si-based electronics in highly efficient devices.

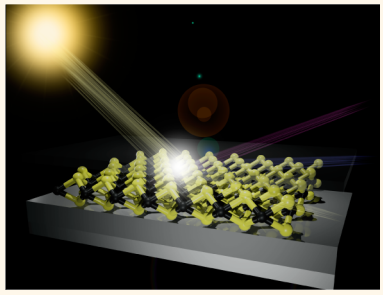

KEYWORDS: molybdenum disulfide · heterojunction solar cell · 2D material · monolayer · chemical vapor deposition

Two-dimensional materials have been widely developed and characterized in recent years due to their promising potential in future electronics. Devices such as transistors, memories, photodetectors, and photocatalyzed hydrogen evolution reactors based on 2D materials have been successfully fabricated.[1−10] For example, monolayer MoS_2 transistors have been demonstrated with on/off ratios of 10^8 and ultralow standby power dissipation.[1] Graphene electrodes have been applied in developing fully transparent resistive memory to suppress undesired surface effects present in oxide memory devices.[2] Photodetectors based on few-layered MoS_2 have exhibited excellent photodetection properties including a high broadband gain up to 24, a high detectivity up to 10^{10} cm $Hz^{1/2}$/W, and a fast photoresponse time of 40 μs.[3,4] In addition, few-layered MoS_2 photodetectors can be operated under working temperatures up to 200 °C and after 2 MeV proton illumination with $\sim 10^{11}$ cm^{-2} fluences, enabling harsh electronic applications.[3,4] Atomically thin graphene−MoS_2 heterostructures have been designed to exhibit a photogain greater than 10^8.[5] Phototransistors based on monolayer MoS_2 have also been reported to exhibit a photoresponsivity as high as 2200 A W^{-1},[6] demonstrating the emerging applications of 2D materials for high-efficiency optoelectronic devices.

In particular, the 2D monolayers of semiconducting transition-metal dichalcogenides (TMDs) have direct band gaps, possessing intriguing optical properties suitable for optoelectronic applications in light-emitting diodes[11] and photovoltaics.[12−14] To realize the highly efficient optoelectronic devices based on the TMD monolayers, it is also important to develop a strategy to tune the band gaps of the TMD monolayers.[15] Amazingly, it has been reported that the 2D TMD materials can absorb up to 5−10% of incident sunlight in a thickness of less than 1 nm and have been shown to achieve 1 order of magnitude higher sunlight absorption than the most commonly used solar absorbers such as GaAs and Si.[12] However, due to the difficulties in fabricating large-scale defect-free 2D TMD materials, the development of 2D TMD-based solar devices is limited. Although few reports have claimed a breakthrough in TMD solar devices, most works use nanosheets, nanoparticles, and bulk forms of the materials rather than 2D materials.[16−18] For example,

* Address correspondence to jrhau.he@kaust.edu.sa, ljchen@mx.nthu.edu.tw.

Received for review May 21, 2014 and accepted July 21, 2014.

Published online July 21, 2014
10.1021/nn502776h

Shanmugan *et al.* have transferred 220 nm thick MoS_2 nanomembranes stacked with Au, creating a Schottky junction at the MoS_2/Au interface to achieve a solar cell efficiency of 1.8%.[16] MoS_2/TiO_2 nanocomposites have been applied in bulk heterojunction solar cells with an efficiency of 1.3%.[17] Recently, WS_2/MoS_2 and MoS_2/graphene monolayer-based solar cells have been reported as the thinnest solar devices with ultrahigh power densities per kilogram.[12,13] However, due to the limited absorption in these fully monolayer-based materials, the efficiencies of MoS_2/graphene and WS_2/MoS_2 monolayer-based solar cells are only ~1 and ~1.5%, respectively, which are unsatisfactory for industrial production.

For practically applicable solar cell design, it is of great importance to develop more cost-effective devices. This can be pursued by either further enhancing the efficiency[19,20] or lowering the cost[21,22] of the device. Both have been achieved in various kinds of Si-based heterojunction solar cells as Si has dominated the commercial photovoltaic market in the past decades due to the high abundance of Si materials, acceptable power conversion efficiencies, and mature Si semiconductor technologies.[19−22] Therefore, apart from pursuing all 2D material-based devices, to realize 2D materials for practical solar energy applications, the integration of atomically thin 2D materials with commercially available materials is desired for high cost effectiveness. In order to achieve the goal, wafer-scale fabrication methods for 2D materials have been provided.[23−25] However, devices based on large-scale monolayer materials have not yet been widely demonstrated due to the limited condition for the direct growth of 2D materials, the challenge for fabricating intact 2D monolayer materials, and the polymer residues induced during the transferring process.

In this work, large-scale MoS_2 monolayers have been successfully fabricated by a chemical vapor deposition (CVD) method.[25] By transferring large-scale monolayer MoS_2, we are able to fabricate a solar cell device with an intact MoS_2 monolayer up to 1 cm × 1 cm in area on the p-Si substrate. To explore the potential of solar systems based on the monolayer MoS_2, it is vital to understand the interfacial band alignment as it determines the photovoltaic efficiency. Thus, ultraviolet photoemission spectroscopy (UPS) has been applied to clearly show the band structure of MoS_2 and p-Si, confirming the creation of a type-II heterojunction between monolayer MoS_2 and p-Si. By designing and fabricating the heterojunction solar cell device, we have achieved a power conversion efficiency of 5.23%, which is the highest efficiency so far for monolayer TMD-based solar cells. The entire process for monolayer TMD-based solar cells demonstrated here takes full advantage of wafer-level, batch processing to minimize cost and leverages the existing Si manufacturing infrastructure to maximize performance, reliability, and scalability.

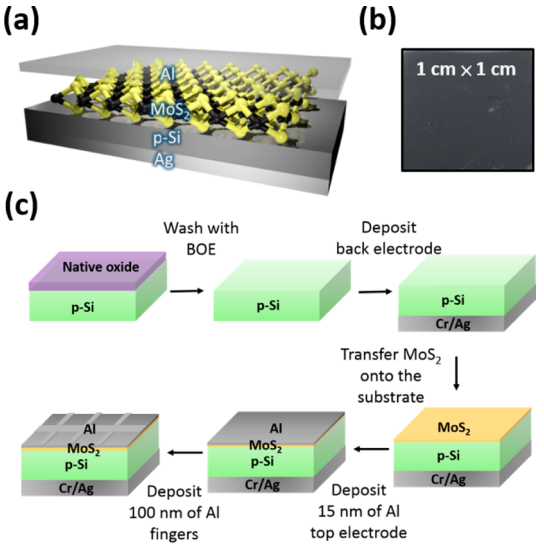

Figure 1. (a) Device structure of MoS_2/p-Si heterojunction solar cell. (b) A 1 cm × 1 cm photographic image of monolayer MoS_2 transferred on p-Si. (c) Fabrication procedure of MoS_2/p-Si heterojunction solar cell.

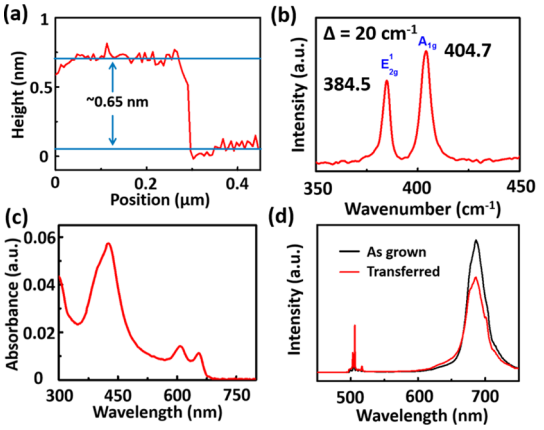

Figure 2. (a) Atomic force microscopy profile and (b) Raman spectrum of monolayer MoS_2. (c) Absorbance spectrum of monolayer MoS_2 on the glass substrate. (d) PL spectra of as-grown and transferred MoS_2.

RESULTS AND DISCUSSION

Figure 1a shows the schematic of the monolayer MoS_2/p-Si device, and Figure 1b shows a photographic image of monolayer MoS_2 transferred on p-Si, indicating its uniformity. The device is fabricated according to the steps shown in Figure 1c. The p-type Si substrate was first immersed in the buffered oxide etchant to remove native oxide layers. Cr/Ag layers of 5 nm/300 nm were deposited as the back electrode. Monolayer MoS_2 was then transferred on top of p-Si. The sample was cut into proper size of about 1 cm × 1 cm with full coverage of monolayer MoS_2 on Si (Figure 1b). Fifteen nanometers of semitransparent and 100 nm of finger-patterned Al were deposited as the top electrode. The thin Al layer was used for creating an ohmic contact with the MoS_2 monolayer to facilitate carrier collection at the top electrodes. Due to the

semitransparent behavior of merely 15 nm thickness, most of the light can still reach the junction of the device. As a comparison, a device with pristine Al/p-Si Schottky junction is fabricated as the control set.

After fabrication and transfer processes, the thickness of the MoS_2 monolayer was characterized. Figure 2a shows the atomic force microscopy (AFM) image of as-transferred MoS_2 on p-Si. The height of the MoS_2 layer is ~0.65 nm, indicating that the single-layer structure of MoS_2 is formed. To further confirm the monolayer characteristic of the MoS_2 layer, Raman spectroscopy measurement was carried out. The energy difference in Raman peaks can be used to determine the layered structure of MoS_2.[26] In Figure 2b, E^1_{2g} and A_{1g} modes of the MoS_2 characteristic peaks are seen at 384.5 and 404.7 cm^{-1}, respectively, indicating that monolayer MoS_2 has been successfully transferred on the p-Si substrate.[26] To further evaluate the optical properties of monolayer MoS_2, absorbance and photoluminescence (PL) measurements have been performed. As shown in Figure 2c, significant light absorption for the wavelengths below 680 nm indicates the presence of a direct optical band gap of monolayer MoS_2 at 1.9 eV. In Figure 2d, the PL spectra of as-grown and transferred MoS_2 monolayers are measured under the excitation of a 473 nm laser. The characteristic peak at 680 nm corresponds to the direct band transition between valence band maximum and conduction band minimum at the K point of the Brillouin zone.[27] The smaller peaks around 500 nm correspond to the Raman scattering peaks of monolayer MoS_2. It is shown that, after transferring onto Si substrates, monolayer MoS_2 retains a strong emission peak, indicating that the monolayer of MoS_2 is still of high quality.

Since the MoS_2 layer is much thinner than the Si substrate, it is critical to analyze the junction existing at the interface of MoS_2/p-Si. To gain insight into the electronic structures of the MoS_2/p-Si heterojunction, we have performed the UPS analysis. The work function can be calculated from the difference between the cutoff of the highest binding energy and the photon energy of the exciting radiation. The valence band maximum can be calculated from the cutoff of the lowest binding energy.[28] As shown in Figure 3a, after covering monolayer MoS_2, the work function of the Si surface has decreased from 4.45 to 4.20 eV. In Figure 3b, the energy difference between the Fermi level and valence band maximum is increased from 0.5 to 1.7 eV, demonstrating the n-type behavior of monolayer MoS_2. Work functions and energy differences between the Fermi level and valence band maximum are summarized in Table 1. On the basis of the above results, we have constructed a band diagram showing the band bending behavior at the monolayer MoS_2 and p-Si interface. The junction forms a type-II heterojunction with a built-in potential that promises

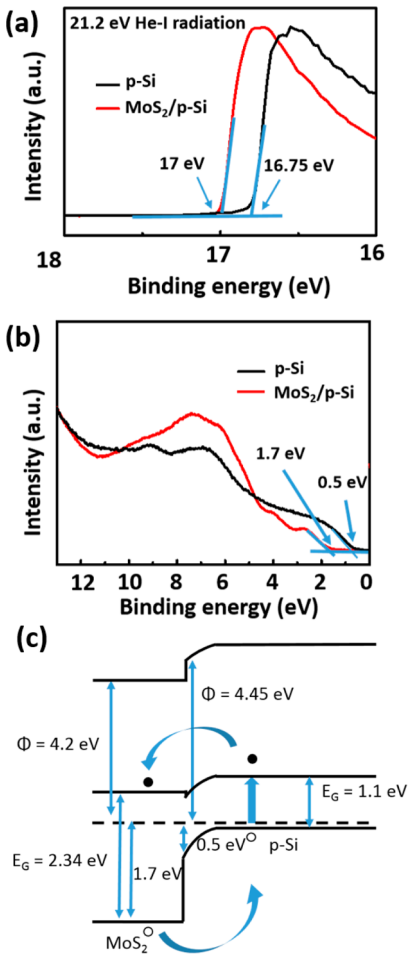

Figure 3. UPS spectra of (a) p-Si and (b) MoS_2/Si. (c) Band diagram of MoS_2/p-Si heterojunction obtained from UPS measurements. Φ is work function, and E_G is energy band gap.

TABLE 1. Work Functions and Energy Differences between Fermi Level and Valence Band Maximum of MoS_2 and p-Si Measured from UPS

	work function (eV)	energy difference (eV)
MoS_2	4.20	1.7
p-Si	4.45	0.5

an excellent photovoltaic performance (Figure 3c), which will be discussed later. In ideal semiconductor device models, the depletion condition/width of the p−n junction is dependent on the doping concentration of semiconductors, dielectric permittivity, built-in voltage, and the applied bias. For MoS_2 monolayer transferred onto the Si substrate, there might be surface detects, interfacial traps, and even a native oxide layer induced, which would deviate from the ideal condition. So far, the physics at the 2D/3D semiconductor interface is still under study. Under biased conditions, whether MoS_2 is fully depleted or not also requires further study since the metal contact on the top might also contribute the depletion phenomenon due to the ultrathin thickness of monolayer MoS_2.

However, it has been observed in recent works that classical diodes and related optoelectronic devices could be prepared using a combination of an atomically thin 2D semiconductor and a 3D semiconductor.[29] It should be noted that by probing the quasiparticle band structure of single-layer MoS_2 using scanning tunneling microscopy and spectroscopy, the quasiparticle band gap is 2.34 eV, which is 0.44 eV larger than the optical band gap, considering the binding energy for exciton.[30] For ideal models, the exciton binding energy of 2D electron−hole plasma is 4 times greater than that in bulk medium.[31] For practical cases, it has also been reported that, in TMDs, the screening effect is reduced and the carrier effective mass is relatively large, and electron−hole interactions are much stronger than in conventional semiconductors.[32] The large interaction indicates a high exciton binding energy in 2D materials.

After device fabrication, we characterized the MoS_2/p-Si solar cell performance. Figure 4a shows the $J-V$ characteristics of the MoS_2/p-Si heterojunction solar cell. The photovoltaic parameters of the device are listed in Table 2. For comparison, Al/p-Si Schottky cells have been fabricated, as shown in Supporting Information Figure S1 and Table S1. It is revealed that, compared with Al/p-Si Schottky solar cells, the Al-contacted monolayer MoS_2/p-Si solar cell shows improved V_{OC} from 0.38 to 0.41 V, J_{SC} from 21.66 to 22.36 mA/cm^2, and FF from 56.02 to 57.26%, giving rise to an efficiency of 5.23%. The improved V_{OC} can be attributed to the formation of heterojunctions at the MoS_2/p-Si interface, inducing a large built-in potential field across the solar cell, which is consistent with UPS measurements. Larger J_{SC} is mainly due to the increased absorption of the MoS_2 monolayer and the formation of the depletion region at the MoS_2/Si interface in which the photoexcited carriers can be possibly separated. Moreover, since the work function of MoS_2 is close to that of Al, the carrier recombination between Al and MoS_2 can be minimized to enhance carrier collection efficiency. Therefore, J_{SC} and FF can be further improved. Accordingly, the MoS_2/p-Si device exhibits an efficiency of 5.23%, which is the highest among all TMD monolayer-based solar cell devices.

Figure 4b shows the external quantum efficiency (EQE) spectrum of the monolayer MoS_2/p-Si heterojunction solar cell. Compared to the Al/p-Si Schottky solar cell (Figure S1b), the monolayer MoS_2-based heterojunction solar cell exhibits broadband enhancement for the wavelengths below 900 nm due to the improved carrier collection efficiency by the addition of the MoS_2 monolayer. For wavelengths below 680 nm, the significant enhancement can be attributed to the increased absorption of the MoS_2 monolayer. Theoretically, although the absorption spectrum shows that MoS_2 monolayer can absorb photons with energy larger than 1.9 eV (653 nm), only photons with energy above 2.34 eV (530 nm) can generate charge

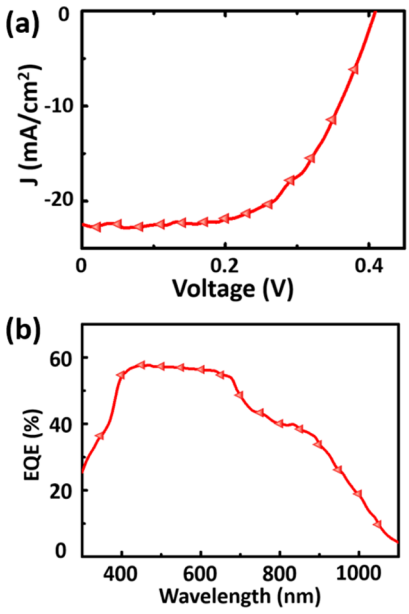

Figure 4. (a) $J-V$ characteristics and (b) EQE spectra of MoS_2/p-Si heterojunction solar cells.

TABLE 2. Photovoltaic Parameters of the MoS_2/p-Si Heterojunction Solar Cell

V_{OC} (V)	J_{SC} (mA/cm^2)	FF (%)	PCE (%)
0.41	22.36	57.26	5.23

carriers in this layer that can be effectively collected by the electrode. However, the absorbed photon between 1.9 and 2.34 eV can also be re-emitted by the MoS_2 monolayer at the MoS_2/Si interface to generate more charge carriers in Si, resulting in the prominent enhancement of EQE. To confirm the light emission behavior in this region, we have measured the PL excitation (PLE) spectrum for wavelengths between 350 and 650 nm of monolayer MoS_2. The PLE spectrum is measured at the emission peak of 676 nm. As shown in Figure S2, the PLE intensity increases with decreasing wavelength below 600 nm. The result indicates that charge carriers generated by photons with energy lower than the quasiparticle band gap of 2.34 eV would recombine immediately to emit light with energy equivalent to the optical band gap of 1.9 eV. To further optimize the performance of MoS_2/p-Si heterojunction cells, the thickness-dependent photovoltaic properties of 2D materials are important, which is under investigation. For multilayer MoS_2, the band gaps are narrowed and should absorb a broader wavelength range of light. However, with more light absorbed in the thin 2D material layer, it could also inhibit light from arriving at the Si layer. We note that in all-2D-material-based schemes, such as graphene−MoS_2 and WSe_2−MoS_2 heterojunctions, using multilayers instead of single layers should be desired and should lead to enhanced absorption in the active region of these devices.

CONCLUSION

We have demonstrated a high-quality monolayer n-type MoS_2 on the p-Si substrate to achieve the highest efficiency of 5.23% among all TMD monolayer-based solar cells. Excellent photovoltaic operation in large-scale MoS_2 monolayers is realized by the formation of a type-II heterojunction with p-Si, creating a built-in electric field near the interface between MoS_2 and p-Si to facilitate photogenerated carrier separation. This work shows that monolayer MoS_2 can be fully integrated into the Si manufacturing process, which holds promise for realizing 2D materials in a variety of Si-based electronic and optical devices.

EXPERIMENTAL SECTION

Large-area monolayer MoS_2 was prepared by CVD in a hot-wall furnace. Direct growth of MoS_2 on p-Si is not applicable due to thick oxide layers formed through the high-temperature process needed for the CVD procedure, preventing MoS_2 from forming a heterojunction with p-Si. Therefore, the multistep growth and transfer process is preferred. The MoO_3 powder was first placed in a ceramic boat, and a sapphire substrate pretreated with aqueous reduced graphene oxide was mounted on the top of the boat. Then a separate boat with sulfur powder was placed neighboring the MoO_3 powder. The chamber was heated to 650 °C in nitrogen ambient environment. MoO_3 powder was reduced by the sulfur vapor to form MoO_{3-x}. Then the compounds diffused to the substrate and further reacted with sulfur vapor to form homogeneous monolayer MoS_2.

After synthesis and characterization, the monolayer MoS_2 on sapphire was spin-coated with PMMA and immersed into NaOH solution. The monolayer was fished out with p-Si substrate, followed by drying out on the hot plate and immersing in acetone for the removal of PMMA. After transferring monolayer MoS_2, the thickness of MoS_2 was revealed by AFM (Veeco Dimension-Icon system). Raman and PL spectra were obtained by confocal Raman microscopic systems (NT-MDT) with a 473 nm laser (spot size ~0.5 μm in diameter). PLE measurements were carried out using a Hitachi F-4500 fluorescence spectrophotometer. The absorption of the monolayer MoS_2 was measured by transferring it onto a glass substrate with a UV−visible−NIR spectrometer (JASCO V-670). To fabricate the MoS_2/p-Si heterojunction solar cell device, we used p-type Si wafers with a diameter of 2 in. and a thickness of 250 μm. The resistivity of the Si wafers is 0.1−0.5 Ωcm, which corresponds to the boron doping concentration between 3.2×10^{16} and 2.5×10^{17} cm^{-3}. The substrates were first cut into smaller pieces to ensure the full coverage of MoS_2 (about 1 cm × 1 cm). Cr/Ag layers of 5 nm/300 nm were thermally evaporated as the back electrode. Then, 15 nm thick Al was deposited on MoS_2 followed by 100 nm thick finger-patterned Al (both thermally evaporated) to form the top electrode. UPS was performed in an ultrahigh vacuum chamber using a helium lamp source emitting at 21.2 eV. *J*−*V* characteristics and EQE spectra were measured by Agilent B2902A precision source/measure unit and Enli R3011 spectral response system, respectively.

Conflict of Interest: The authors declare no competing financial interest.

Supporting Information Available: J−*V* characteristics and EQE spectra of Al/p-Si Schottky solar cell; PLE spectrum of monolayer MoS_2; photovoltaic parameters of Al/p-Si Schottky solar cell. This material is available free of charge *via* the Internet at http://pubs.acs.org.

REFERENCES AND NOTES

1. Radisavljevic, B.; Radenovic, A.; Brivio, J.; Giacometti, V.; Kis, A. Single-Layer MoS_2 Transistors. *Nat. Nanotechnol.* **2011**, *6*, 147–150.
2. Yang, P. K.; Chang, W. Y.; Teng, P. Y.; Jeng, S. F.; Lin, S. J.; Chiu, P. W.; He, J. H. Fully Transparent Resistive Memory Employing Graphene Electrodes for Eliminating Undesired Surface Effects. *Proc. IEEE* **2013**, *101*, 1732–1739.
3. Tsai, D. S.; Liu, K. K.; Lien, D. H.; Tsai, M. L.; Kang, C. F.; Lin, C. A.; Li, L. J.; He, J. H. Few-Layer MoS_2 with High Broadband Photogain and Fast Optical Switching for Use in Harsh Environments. *ACS Nano* **2013**, *7*, 3905–3911.
4. Tsai, D. S.; Lien, D. H.; Tsai, M. L.; Su, S. H.; Chen, K. M.; Ke, J. J.; Yu, Y. C.; Li, L. J.; He, J. H. Trilayered MoS_2 Metal-Semiconductor-Metal Photodetectors: Photogain and Radiation Resistance. *IEEE Sel. Top. Quantum Electron.* **2014**, *20*, 3800206.
5. Zhang, W.; Chu, C. P.; Huang, J. K.; Chen, C. H.; Tsai, M. L.; Chang, Y. H.; Liang, C. T.; Chen, Y. Z.; Chueh, Y. L.; He, J. H.; *et al.* Ultrahigh-Gain Photodetectors Based on Atomically Thin Graphene−MoS_2 Heterostructures. *Sci. Rep.* **2014**, *4*, 3826.
6. Zhang, W.; Huang, J. K.; Chen, C. H.; Chang, Y. H.; Cheng, Y. J.; Li, L. J. High-Gain Phototransistors Based on a CVD MoS_2 Monolayer. *Adv. Mater.* **2013**, *25*, 3456–3461.
7. Xiang, Q.; Yu, J.; Jaroniec, M. Synergetic Effect of MoS_2 and Graphene as Cocatalysts for Enhanced Photocatalytic H_2 Production Activity of TiO_2 Nanoparticles. *J. Am. Chem. Soc.* **2012**, *134*, 6575–6578.
8. Hou, Y.; Laursen, A. B.; Zhang, J.; Zhang, G.; Zhu, Y.; Wang, X.; Dahl, S.; Chorkendorff, I. Layered Nanojunctions for Hydrogen-Evolution Catalysis. *Angew. Chem., Int. Ed.* **2013**, *52*, 3621–3625.
9. Wang, H.; Lu, Z.; Kong, D.; Sun, J.; Hymel, T. M.; Cui, Y. Electrochemical Tuning of MoS_2 Nanoparticles on Three-Dimensional Substrate for Efficient Hydrogen Evolution. *ACS Nano* **2014**, *8*, 4940–4947.
10. Chuang, S.; Battaglia, C.; Azcatl, A.; McDonnell, S.; Kang, J. S.; Yin, X.; Tosun, M.; Kapadia, R.; Fang, H.; Wallace, R. M.; *et al.* MoS_2 p-Type Transistors and Diodes Enabled by High Work Function MoO_x Contacts. *Nano Lett.* **2014**, *14*, 1337–1342.
11. Ross, J. S.; Klement, P.; Jones, A. M.; Ghimire, N. J.; Yan, J.; Mandrus, D. G.; Taniguchi, T.; Watanabe, K.; Kitamura, K.; Yao, W.; *et al.* Electrically Tunable Excitonic Light-Emitting Diodes Based on Monolayer WSe_2 p−n Junctions. *Nat. Nanotechnol.* **2014**, *9*, 268–272.
12. Bernardi, M.; Palummo, M.; Grossman, J. C. Extraordinary Sunlight Absorption and One Nanometer Thick Photovoltaics Using Two-Dimensional Monolayer Materials. *Nano Lett.* **2013**, *13*, 3664–3670.
13. Gan, L. Y.; Zhang, Q.; Cheng, Y.; Schwingenschlögl, U. Photovoltaic Heterojunctions of Fullerenes with MoS_2 and WS_2 Monolayers. *J. Phys. Chem. Lett.* **2014**, *5*, 1445–1449.
14. Feng, J.; Qian, X.; Huang, C. W.; Li, J. Strain-Engineered Artificial Atom as a Broad-Spectrum Solar Energy Funnel. *Nat. Photonics* **2012**, *6*, 866–872.
15. Su, S. H.; Hsu, Y. T.; Chang, Y. H.; Chiu, M. H.; Hsu, C. L.; Hsu, W. T.; Chang, W. H.; He, J. H.; Li, L. J. Band Gap-Tunable Molybdenum Sulfide Selenide Monolayer Alloy. *Small* **2014**, *10*, 2589–2594.
16. Shanmugam, M.; Durcan, C. A.; Yu, B. Layered Semiconductor Molybdenum Disulfide Nanomembrane Based Schottky-Barrier Solar Cells. *Nanoscale* **2012**, *4*, 7399–7405.
17. Shanmugam, M.; Bansal, T.; Durcan, C. A.; Yu, B. Molybdenum Disulphide/Titanium Dioxide Nanocomposite-Poly 3-hexythiophene Bulk Heterojunction Solar Cell. *Appl. Phys. Lett.* **2012**, *100*, 153901.
18. Gu, X.; Cui, W.; Li, H.; Wu, Z.; Zeng, Z.; Lee, S. T.; Zhang, H.; Sun, B. A Solution-Processed Hole Extraction Layer Made

from Ultrathin MoS_2 Nanosheets for Efficient Organic Solar Cells. *Adv. Energy Mater.* **2013**, *3*, 1262–1268.
19. Wang, H. P.; Lin, T. Y.; Hsu, C. W.; Tsai, M. L.; Huang, C. H.; Wei, W. R.; Huang, M. Y.; Chien, Y. J.; Yang, P. C.; Liu, C. W.; *et al.* Realizing High-Efficiency Omnidirectional n-Type Si Solar Cells *via* the Hierarchical Architecture Concept with Radial Junctions. *ACS Nano* **2013**, *7*, 9325–9335.
20. Wang, H. P.; Lin, T. Y.; Tsai, M. L.; Tu, W. C.; Huang, M. Y.; Yang, P. C.; Chien, Y. J.; Liu, C. W.; Chueh, Y. L.; He, J. H. Toward Efficient and Omnidirectional n-Type Si Solar Cells: Concurrent Improvement in Optical and Electrical Characteristics by Employing Microscale Hierarchical Structures Consisting of Grooves and Pyramids. *ACS Nano* **2014**, *8*, 2659–2669.
21. Tsai, S. H.; Chang, H. C.; Wang, H. H.; Chen, S. Y.; Lin, C. A.; Chen, S. A.; Chueh, Y. L.; He, J. H. Significant Efficiency Enhancement of Hybrid Solar Cells Using Core–Shell Nanowire Geometry for Energy Harvesting. *ACS Nano* **2011**, *5*, 9501–9510.
22. Wei, W. R.; Tsai, M. L.; Ho, S. T.; Tai, S. H.; Ho, C. R.; Tsai, S. H.; Liu, C. W.; Chung, R. J.; He, J. H. Above-11%-Efficiency Organic–Inorganic Hybrid Solar Cells with Omnidirectional Harvesting Characteristics by Employing Hierarchical Photon-Trapping Structures. *Nano Lett.* **2013**, *13*, 3658–3663.
23. Liu, K. K.; Zhang, W.; Lee, Y. H.; Lin, Y. C.; Chang, M. T.; Su, C. Y.; Chang, C. S.; Li, H.; Shi, Y.; Zhang, H.; *et al.* Growth of Large-Area and Highly Crystalline MoS_2 Thin Layers on Insulating Substrates. *Nano Lett.* **2012**, *12*, 1538–1544.
24. Lee, Y. H.; Zhang, X. Q.; Zhang, W.; Chang, M. T.; Lin, C. T.; Chang, K. D.; Yu, Y. C.; Wang, J. T. W.; Chang, C. S.; Li, L. J.; *et al.* Synthesis of Large-Area MoS_2 Atomic Layers with Chemical Vapor Deposition. *Adv. Mater.* **2012**, *24*, 2320–2325.
25. Lin, Y. C.; Zhang, W.; Huang, J. K.; Liu, K. K.; Lee, Y. H.; Liang, C. T.; Chu, C. W.; Li, L. J. Wafer-Scale MoS_2 Thin Layers Prepared by MoO_3 Sulfurization. *Nanoscale* **2012**, *4*, 6637–6641.
26. Li, H.; Zhang, Q.; Yap, C. C. R.; Tay, B. K.; Edwin, T. H. T.; Olivier, A.; Baillargeat, D. From Bulk to Monolayer MoS_2: Evolution of Raman Scattering. *Adv. Funct. Mater.* **2012**, *22*, 1385–1390.
27. Mak, K. F.; Lee, C.; Hone, J.; Shan, H.; Heinz, T. F. Atomically Thin MoS_2: A New Direct-Gap Semiconductor. *Phys. Rev. Lett.* **2010**, *105*, 136805.
28. Rabalais, J. W. *Principles of Ultraviolet Photoelectron Spectroscopy*; Wiley: New York, 1977.
29. Lopez-Sanchez, O.; Llado, E. A.; Koman, V.; i Morral, A. F.; Radenovic, A.; Kis, A. Light Generation and Harvesting in a van der Waals Heterostructure. *ACS Nano* **2014**, *8*, 3042–3048.
30. Zhang, C.; Johnson, A.; Hsu, C. L.; Li, L. J.; Shih, C. K. Direct Imaging of Band Profile in Single Layer MoS_2 on Graphite: Quasiparticle Energy Gap, Metallic Edge States and Edge Band Bending. *Nano Lett.* **2014**, *14*, 2443–2447.
31. Haug, H.; Koch, S. W. *Quantum Theory of the Optical and Electronic Properties of Semiconductors*, 5th ed.; World Scientific: River Edge, NJ, 2009.
32. Ross, J. S.; Klement, P.; Jones, A. M.; Ghimire, N. J.; Yan, J.; Mandrus, D. G.; Taniguchi, T.; Watanabe, K.; Kitamura, K.; Yao, W.; *et al.* Electrically Tunable Excitonic Light-Emitting Diodes Based on Monolayer WSe_2 p–n Junctions. *Nat. Nanotechnol.* **2014**, *9*, 268–272.